A comparative experimental study on the hydrodynamic performance of two floating solar structures with a breakwater in waves

Yifeng Yang [a,b], Chenhao Mi [a], Binjian Ou [a], Anson Wong [c], John Gordon Duffy [c], Tim Wood [d], IKAP Utama [e], Wenchuang Chen [f,*], Luofeng Huang [a,*]

[a] *Faculty of Engineering and Applied Sciences, Cranfield University, Cranfield, MK43 0AL, United Kingdom*
[b] *Department of Mechanical Engineering, University College London, London, WC1E 7JE, United Kingdom*
[c] *DuPont, 1501 Larkin Center Drive, Midland, MI, 48642, United States of America*
[d] *Achelous Energy Limited, Unit 2 Black Robins Farm, Edenbridge, TN8 6QP, United Kingdom*
[e] *Department of Naval Architecture, Institut Teknologi Sepuluh Nopember, Surabaya, 60111, Indonesia*
[f] *School of Civil Engineering, Sun Yat-Sen University, Zhuhai, 519082, China*

ARTICLE INFO

ABSTRACT

Floating Photovoltaic (FPV) is considered as a highly promising clean energy solution. In recent years, FPV has been widely deployed in calm water around the world. However, to find available space for further expansion, FPV needs to be deployed in seas whilst the oceanic waves significantly influence the structural stability and energy performance. On one hand, wave loads may cause structural fatigue and damage. On the other hand, wave-induced rotations of a floating solar panel will vary its tilt angle to the sunlight and thus affect the power output. To explore the new research field of ocean-based FPV, this work first designed a novel catamaran FPV floater with a four-point mooring system. Comparative experiments were then conducted in a wave tank to compare its seakeeping ability with a conventional flat-plate floater. Besides, a breakwater structure was further introduced to enhance the stability of these two types of floaters. Detailed data on floater motions and mooring line forces were collected under monochromatic wave conditions. Extensive analysis was performed to evaluate the wave-mitigating performance of the breakwater, as well as the nonlinearity in the motion and force time histories. Overall, the work provides valuable experimental data and novel insights into the design of FPV floaters and breakwater protection, supporting long-term sustainability of FPV on the ocean.

1. Introduction

The PhotoVoltaic (PV) technology is considered as one of the most promising renewable energy systems for reducing carbon emissions and mitigating climate changes [1]. Normally, solar PV power generation is proportional to its deployment surface area, which may have limited potential in some regions with scarce land resources. Alternatively, we may deploy solar panels on the water surface, which is named Floating PV (FPV) [2]. FPV deployment on calm water is also limited due to the environmental reservation requirement of lakes and reservoirs. However, there is abundant space in coastal and offshore seas, signifying enormous potential [3–5]. In order to deploy FPV on the ocean, it is necessary to understand its hydrodynamic performance in ocean waves.

Substantial studies have indicated that the tilt angle of photovoltaics significantly influences the amount of sunlight absorbed, directly affecting the energy output. For land-based PV systems, the optimal tilt angle can be determined by geographical and environmental factors, and

then this angle can be mechanically fixed upon installation [6–8]. By contrast, the tilt angle of ocean-based FPV systems is further influenced by wave-induced motion. As studied in [9,10], a significant percentage of energy could be lost due to the wave-induced motion of FPV. This motivated research to minimise wave-induced motions based on the designing of floating structures and the usage of the breakwater. On the other hand, wave loads may also cause damage to the structure of FPV systems [11–13], highlighting the need to mitigate wave impacts.

A common FPV structure can consist of three parts, namely the floater, the solar PV module and the mooring system [14,15]. The floater is the major component of the system. Generally, a floater is placed underneath a solar panel, providing buoyancy to support the superstructure of the system, and the floater design is vital for the overall hydrodynamic performance [2,16,17]. Besides, the stability of the system is aided by a bespoke mooring system.

In the past, there has been certain experimental, analytical and numerical works about water wave interaction with FPV systems. For
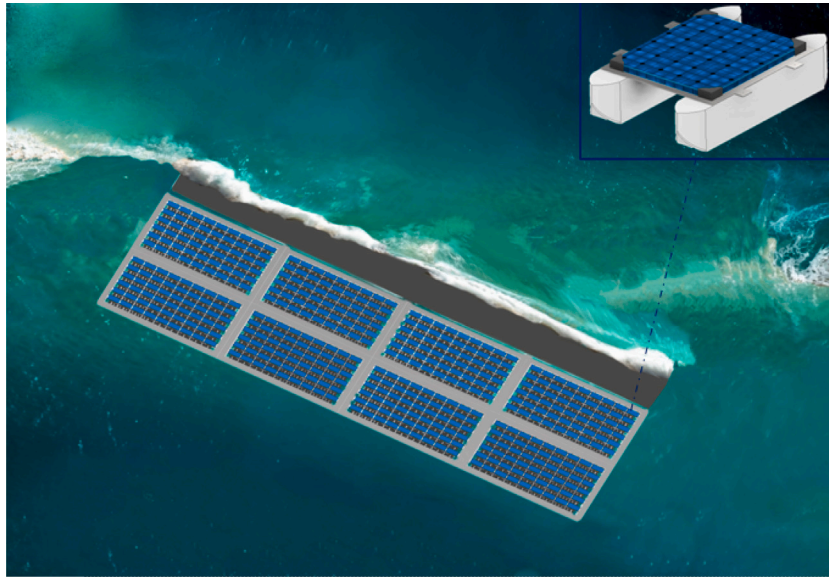

Fig. 1. Visualisation for the application of breakwater upstream a floating solar farm.

experimental studies, Hu et al. [18] proposed a conceptual design of a semi-submergible platform of a triangle configuration, where wind turbines were installed at the three vortexes of the triangle, and the structure had a large deck space to install solar panels. They also conducted a model test in a towing tank with a 1/50 scale to study the hydrodynamic performance of this platform. Choi and Lee [19] investigated the influence of wave loads on FPV systems using finite element analysis, based on which, a 20 kW experimental FPV system was designed and built. Later, Qu et al. [20] proposed a hybrid floating system based on a modular buoyancy-distributed floating foundation, and conducted 1/10 scale ratio hydrodynamic experiments in a deep-water basin, the hydrodynamic performance in regular waves was evaluated. Lee et al. [21] carried out an experiment for a solar farm model, which consisted of 4 units and each unit contained 9 solar panels. In the experiment, regular waves with two incident angles were considered, and it was found that the heave and pitch motions of the floating structure were most dominant, the motion of the entire structure was complex due to the hinged connection of each unit. Delacroix et al. [12] performed an experimental study for a 1:1 scale float system, which was composed of 16 floating modules to support solar panels and 3 footpaths. In their experiment, both the regular and irregular wave conditions were considered, and a specific wave resonant mode was always observed in the pitch motion, even in the narrow wave spectrum. Friel et al. [22] experimentally investigated the wave loads and structural motion of two semi-fixed and semi-immersed horizontal cylinder types of solar panel systems. A physical 1:4.5 scale is used for the test. Similar to Delacroix et al. [12], both the regular and irregular waves were generated to interact with the structures. In their work, the wave force spectral responses of the structure, and the wave attenuation were evaluated to understand the hydrodynamic properties of such floating solar panel configurations. Besides, Jiang et al. [23] proposed a soft-connected lattice-structured FPV model, and conducted experiments for 1:60 scaled model tests for a 2 by 3 array under regular and irregular wave conditions. In addition to the works listed above, other experimental studies can also be found in [23–27].

Apart from physical model tests, there is also a number of works about wave interaction with FPV based on analytical approaches and numerical simulations. For floating solar farms covering a large horizontal area of open water, its motion can be described by the elastic thin plate theory [28] and the fluid can be modelled by using the linearised velocity potential theory. Based on this, Bi and Law [29] investigated the wave interaction with an FPV system with multiple internal hinged points. Zhang et al. [30] studied the wave resonance phenomenon of multi-patch FPV in ocean environments with a stepped seabed. Yang et al. [31] considered the wave interaction with multiple floating solar panels with arbitrary types of constraints. Other similar attempts can be also found in [32,33]. In addition to applying the elastic thin plate theory for the entire floating solar farm, another method is to model each solar panel as a single rigid plate unit. As an example, Wei et al. [15] studied the motion characteristics of multiple types of FPV arrays using computational simulations.

In addition, a breakwater can be a very useful addition to a floating solar farm. A breakwater applied upstream FPV can mitigate direct wave interaction with solar units, as illustrated in Fig. 1. Commonly applied in coastal engineering, a breakwater structure will interact with incoming waves, inducing waves to become splashing water and lose continuity [34,35]. In this way, waves can only radiate a short distance behind the breakwater and have minimal interaction with FPV, so as to minimise the FPV loads and motions. The additional building cost would not be significant with respect to calm-water FPV, as the main additional component is the breakwater in the barrier, i.e. the cost does not increase proportionally with the surface coverage. Thus the larger the surface area of the solar farm, the cheaper the average energy cost will be, potentially supporting large-scale FPV projects [4,13]. Moreover, breakwaters could also be further applied as wave energy converters, so that they not only protect FPV but also generate extra energy [3,36–38]. Therefore it is of great interest to experimentally test a breakwater's effect on FPV loads and motions, which is still a contemporary research gap and will be addressed in this paper.

Although previous experimental works have been conducted to test the hydrodynamic performance of conventional FPV floaters, most of the existing designs are for calm water conditions without ocean waves. To meet the development requirement of coastal and offshore FPV, one of the key challenges in this field is how to design the geometry of floaters with strong seakeeping ability, which still requires further investigation at the current stage. Additionally, to the best of our knowledge, no research has studied the hydrodynamic performance of a combined FPV and breakwater system, especially the wave-mitigating performance remains unclear. As a result, in this paper, a novel catamaran floater is proposed, which is motivated by the strong seakeeping ability of catamaran-type ships [39]. After that, comparative experiments of the catamaran structure are conducted with the conventional flat-plate floater to study their hydrodynamic performance in waves. The experiment is conducted in the wave tank at
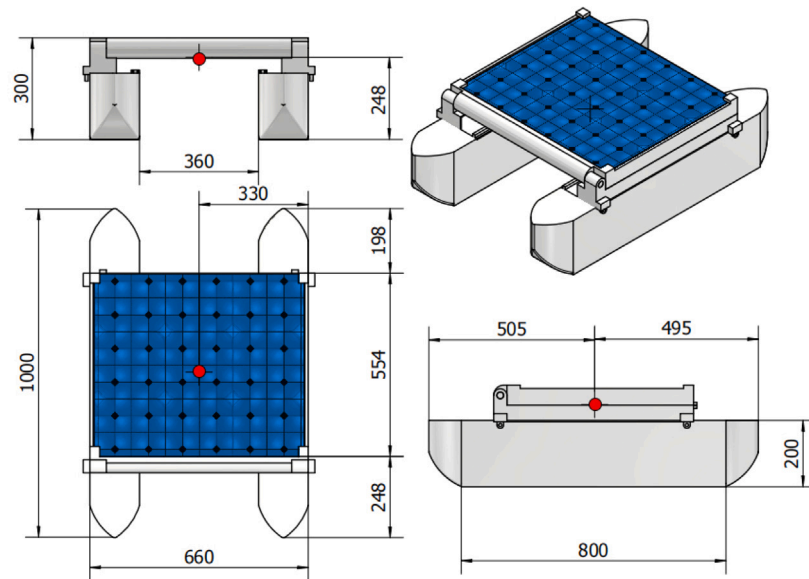
Fig. 2. The sketch of the geometry of the catamaran structure (Length unit: mm); The red point denotes the centre of gravity of the structure.

Cranfield University using monochromatic wave conditions. Moreover, the comparative study integrates a breakwater structure. By measuring the motions of the floaters as well as the mooring line forces, with and without the breakwater, the wave-mitigating performance of the breakwater is evaluated quantitatively. The collected data here in the wave tank can be used to reflect the hydrodynamic properties of FPV in real ocean environments by the Froude scaling rule [40], which aims to provide engineering insights into the design of FPV on seas. Moreover, the nonlinearity in the time histories of motions and forces is also discussed, which offers a comprehensive understanding of the hydrodynamic properties of such types of FPV in waves.

The rest of the paper is organised as follows. The design of two floaters for fitting a standard solar panel is introduced in Section 2. The experimental details, including the experimental facilities, the mooring setup and the breakwater, and the tested wave conditions are discussed in Sections 3.1–3.3 respectively. The experimental results are analysed in Section 4. Finally, conclusions are made in Section 5, along with recommendations for future work.

2. Design of two floaters for fitting a standard solar panel

In this experimental study, two types of floating structures are designed and constrcuted to carry the solar panel, namely a catamaran and a flat plate. The geometries and dimensions of these two types of solar panel structures are given in Figs. 2 and 3 respectively. Both of the structures consist of two parts, namely the floater and a standard solar panel. The standard solar panel for both floaters is the same, with the dimensions of 660 mm×554 mm×100 mm. The floating structure of the catamaran consists of two identical hulls with curved front and rear surfaces, and they are arranged in parallel with the distance between the two inner side walls is 360 mm, as illustrated in Fig. 2. The total occupied volume of the catamaran is 1000 mm × 660 mm × 200 mm. By contrast, the geometry of the flat plate is cuboid with the size of 1000 mm × 660 mm × 200 mm, as shown in Fig. 3. Furthermore, The centres of gravity of these two types of structures are marked as red points in Figs. 2 and 3. Hence, the two floaters make a comparative study, with the flat-plate shape commonly used in conventional FPV and the catamaran being a novel design tested here. It is expected that the catamaran will offer better hydrodynamic performance than the flat plate in certain wave conditions (e.g., lower drag and motion amplitudes) [41], and the present work will evaluate this hypothesis.

The floaters use an Extruded Polystyrene (XPS) foam material, which offers appropriate mechanical strength, buoyancy, water resistance, weatherability, as well as dimensional stability — the XPS has a density of 38 kg/m³ and a compressive strength of 65 psi. The PV panel is a common commercial type, made by TDG Holding Co., Ltd and the model number is T050M365. It applies the monocrystalline cell technology with a maximum power output of 50 W. The connection between the floaters and the PV panel was made by High-Density PolyEthylene (HDPE), with a density of 950 kg/m³. The total weights of the catamaran and flat plate structures are 11.53 kg and 15.23 kg, and the draughts are 6.6 cm and 2.3 cm respectively.

3. Experimental setup

3.1. Wave tank

The experiments were set up at the wave tank of Cranfield University. As shown in Fig. 4(a), the wave tank is 30 m long, 1.5 m wide, and it was filled with fresh water of 1.5 m. At one side of the wave tank, a 3-paddle Edinburgh Design wavemaker was installed to generate waves, while a full-width parabolic beach is fitted across the tank at the other side to absorb waves, which avoids wave reflection and mimics an open sea environment in the middle of the tank. The tank is designed to generate regular waves with frequency ranging from 0.1 to 1.1 Hz, and wave height less than 28 cm. The tested experimental structure was a floating solar unit placed nearly at the centre position of the tank. The distance between both sides of the solar panel device with the tank walls is 42 cm, which is designed to avoid undesirable side-wall reflection that could influence the structural hydrodynamics.

3.2. Moorign systems and the breakwater

In the experiments, both the floating solar unit structures, i.e. the flat plate and catamaran devices, were connected to the bottom of the tank by using four mooring lines. Each of the mooring lines is composed of a spring and a high-tension fishing line, where each spring has an identical original static length of 18.3 cm, and its stiffness is measured to be 454.5 N/m. The total length of each mooring line is 220 cm. Four mooring lines together with the four identical force sensors are used to connect the four corners of the solar panel unit and the bottom of the tank, as shown in Fig. 4(b) and (c). The longitudinal distance or the distance along the tank length direction of the moored point
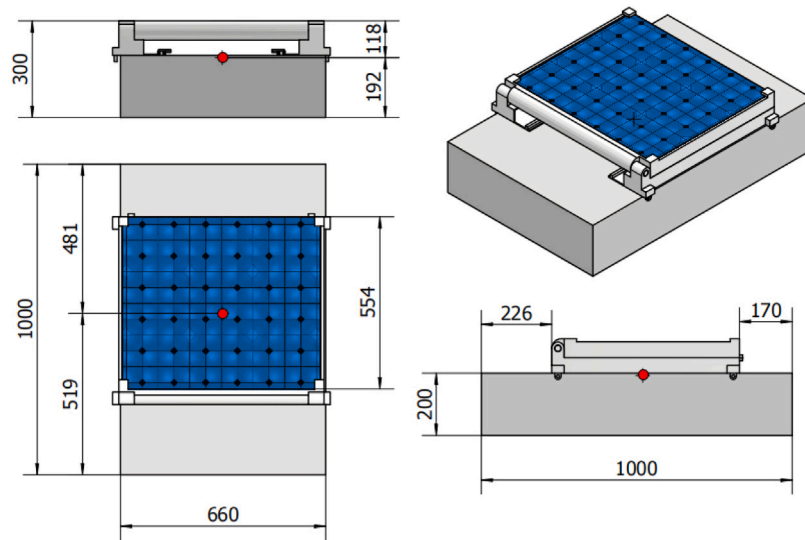
Fig. 3. The sketch of the geometry of the flat plate structure (Length unit: mm); The red point denotes the centre of gravity of the structure.
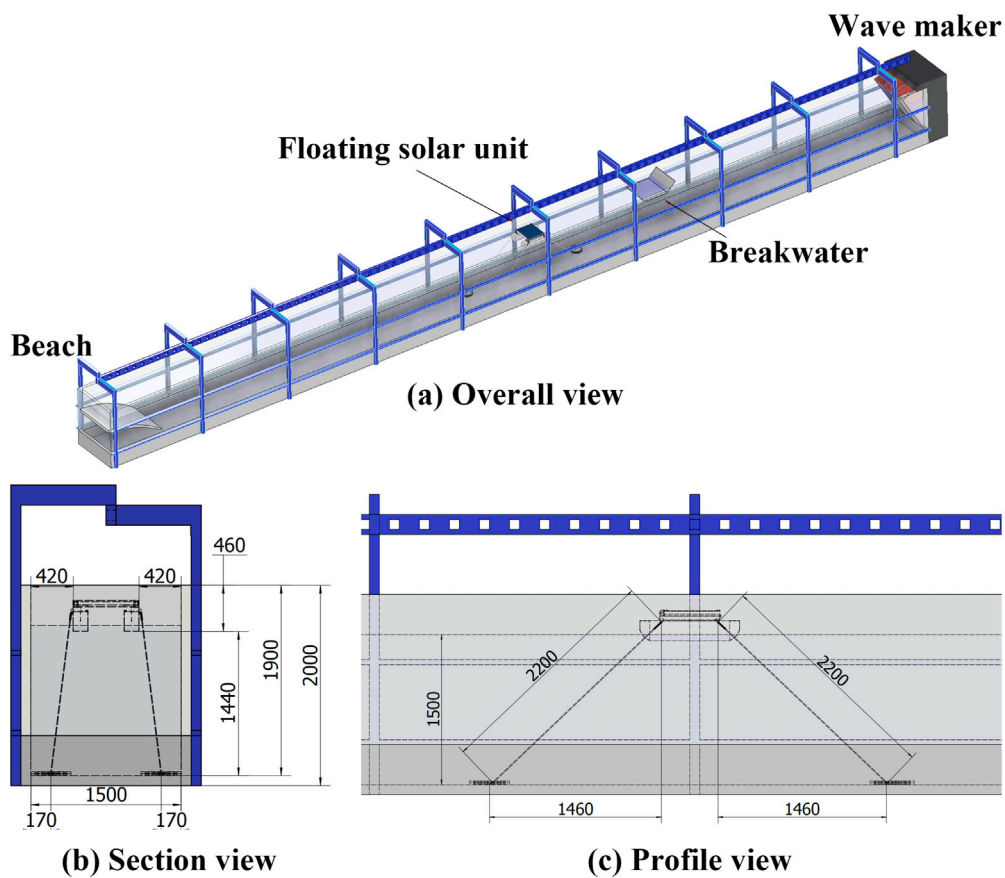

Fig. 4. The sketch of the experimental facility: wave tank, floating solar unit, and the mooring system (dimension unit: mm). (a) Overall view; (b) Section view; (c) Profile view.

at the body and the bottom was designed and measured to be 150 cm. Four mooring lines were arranged in symmetrical positions, so as to avoid the motions (roll, yaw and sway) of the body caused by asymmetrical factors. After the mooring lines were arranged, the pre-tension of each spring was measured by the connected force sensor. Through fine-tuning the position of the moored points on the bottom of the tank, the pre-tensions of the four mooring lines were kept the same. Specifically, for the flat plate device, the preload was measured to be 16.864 N, and for the catamaran device, the preload was measured to be 18.720 N. It should be noted that the slight difference in the preloads between the two devices here is due to the difference in the draught. In such a case, all the springs were subjected to an identical
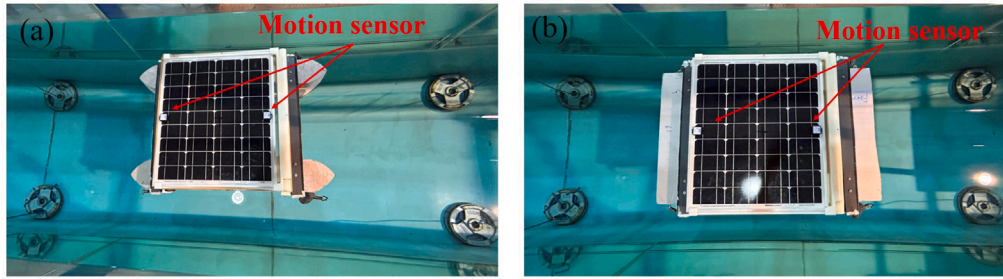
Fig. 5. Photos of two floating solar structures in the tank: (a) Catamaran; (b) Flat plate.

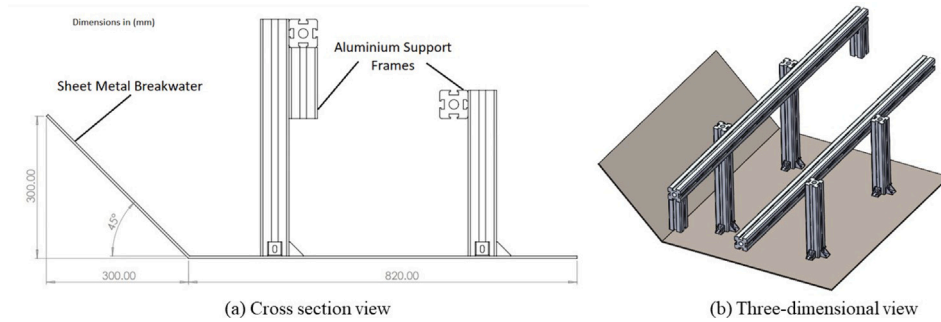(a) Cross section view   (b) Three-dimensional view

Fig. 6. Geometry of the breakwater. (a) Cross section view; (b) Three-dimensional view.

initial tension, which ensured that the mooring lines were in a stretched state.

During the experiments, motion-tracking sensors were used to measure the six-degree freedom motions of the body. Two motion sensors are placed along the longitudinal centreline of the solar panel unit, as shown in Fig. 5. Once data is collected, the motion at the centre of gravity of the body was calculated using the kinematic motion equations of a rigid body [42], together with the coordinates of points of sensors and centre of gravity. Besides, as mentioned above, the forces in the mooring lines were also measured using load cells. Apart from the facilities introduced above, a breakwater was another significant component employed in this study, which is to reduce the impact of water waves on structures. A rectangular breakwater with a 45º bending plate was used, as shown in Fig. 6. The entire plate is connected to the tank by using two support frames. The effective length of the breakwater is designed to be 112 cm. The width of the breakwater is 1 m The breakwater was made of aluminium frames. Besides, when deploying the breakwater in the tank, the distance between the front side of the solar panel structure and the rear side of the breakwater was kept at 2 m, and the breakwater is arranged in a position symmetric about the longitudinal centre line of the tank.

3.3. Tested wave conditions

In the experiments, five wave frequencies, $f = 0.6, 0.7, 0.8, 0.9$ and 1.0 Hz, as well as two wave heights, $H = 5.0$ and 10.0 cm were tested. Hence, there were a total of 10 wave conditions, in combination with 2 floating solar structures, and with and without a breakwater — forming 40 experiments in total. The wavelength can be estimated using the dispersion relation of linear wave theory [43], according to:

$$\frac{2\pi}{\lambda} \tanh\left(\frac{2\pi h}{\lambda}\right) = \frac{\omega^2}{g}, \tag{1}$$

where λ denotes the wavelength, $g = 9.81$ m/s² represents the acceleration due to gravity, $\omega = 2\pi f$ is the angular frequency, and $h = 1.5$ m is the mean water depth of the tank. Based on the data provided above and Eq. (1), the tested wave conditions in this study are summarised in Table 1.

Table 1
Incident wave conditions in the experiment.

Wave condition No.	Wave height (cm)	Wave frequency (Hz)	Wavelength (m)
1	5.0	1.0	1.561
2	5.0	0.9	1.927
3	5.0	0.8	2.437
4	5.0	0.7	3.170
5	5.0	0.6	4.237
6	10.0	1.0	1.561
7	10.0	0.9	1.927
8	10.0	0.8	2.437
9	10.0	0.7	3.170
10	10.0	0.6	4.237

4. Results and discussion

When performing the experiments, all the measurements and cases were repeated twice to ensure the accuracy of the collected data, while almost identical results were observed during all the repeated tests. Hence, valid data were taken only when the floating structure started to move periodically, and average results of five wave circles were taken to calculate relevant amplitudes.

4.1. Wave induced motions

The wave induced motions of the floating solar structures are presented here in the form of heave, pitch, and surge motions, and the corresponding amplitudes are described through the Response Amplitude Operators (RAOs), which quantify the ratio of the motion amplitudes of a floating body to the inciting amplitudes within the incident waves. As defined in [44], we have

$$\text{RAO}_{\text{heave}} = \frac{A_z}{A}, \tag{2a}$$

$$\text{RAO}_{\text{pitch}} = \frac{\Theta_y}{kA}, \tag{2b}$$

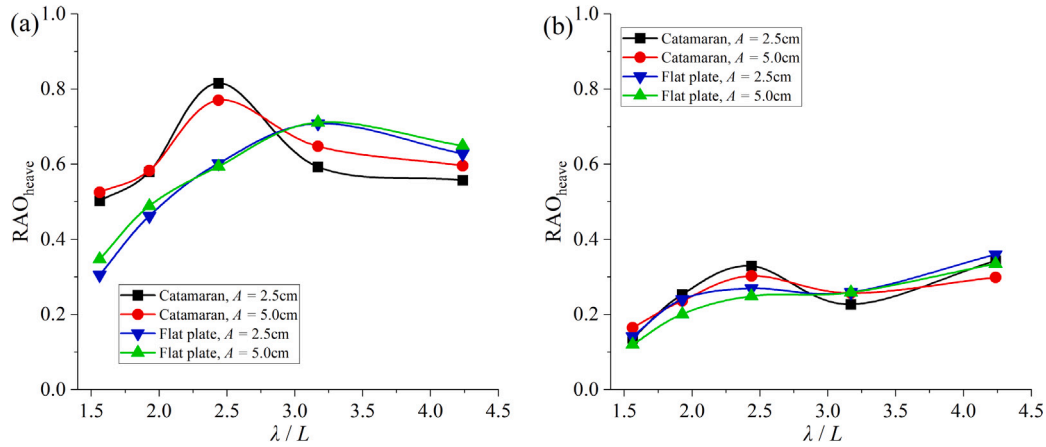$$\text{RAO}_{\text{surge}} = \frac{A_x}{A \cosh kh}, \tag{2c}$$

Fig. 7. Heave motion of the solar panel structures. (a) Without breakwater; (b) With breakwater. Scatters measured from the experiments; Solid lines are the fitted lines from the experimental data.

Table 2
The reduction of RAO_{heave} for the flat plate after the breakwater is used under $A = 5$ cm.

λ/L	Without breakwater	With breakwater	Reduction
4.237	0.649	0.335	48.4%
3.170	0.711	0.259	63.4%
2.437	0.594	0.249	58.2%
1.927	0.488	0.200	59.0%
1.561	0.347	0.120	65.4%

Table 3
The reduction of RAO_{heave} for the catamaran after the breakwater is used under $A = 5$ cm.

λ/L	Without breakwater	With breakwater	Reduction
4.237	0.596	0.299	49.9%
3.170	0.648	0.257	60.4%
2.437	0.770	0.303	60.7%
1.927	0.583	0.236	59.5%
1.561	0.525	0.167	68.6%

Table 4
The reduction of RAO_{pitch} for the flat plate after the breakwater is used under $A = 5$ cm.

λ/L	Without breakwater	With breakwater	Reduction
4.237	0.492	0.277	43.68%
3.170	0.586	0.222	62.18%
2.437	0.542	0.218	59.82%
1.927	0.404	0.152	62.49%
1.561	0.246	0.0864	64.83%

Table 5
The reduction of RAO_{pitch} for the catamaran after the breakwater is used under $A = 5$ cm.

λ/L	Without breakwater	With breakwater	Reduction
4.237	0.215	0.170	20.97%
3.170	0.584	0.200	65.79%
2.437	0.869	0.360	58.50%
1.927	0.560	0.237	57.68%
1.561	0.360	0.0976	72.92%

where $A = H/2$ represents the amplitude of the incident wave, H denotes the wave height as defined in Section 3.3, $k = 2\pi/\lambda$ denotes the wavenumber, A_z, Θ_y and A_x are the amplitudes of the heave, pitch and surge motions respectively.

The results of RAO_{heave} versus the nondimensional wavelength λ/L is given in Fig. 7, where $L = 1.0$ m is the length scale of the structure. In Fig. 7(a), at a fixed λ/L, RAO_{heave} of the flat plate case is quite similar under two amplitudes A. By contrast, obvious differences are observed in RAO_{heave} at $\lambda/L = 2.437, 3.170$ and 4.237 ($f = 0.8, 0.7$ and 0.6 Hz correspondingly) for the catamaran. Besides, under the five considered wavelength, the catamaran has the maximum RAO_{heave} at $\lambda/L = 2.437$ ($f = 0.8$ Hz) with $RAO_{heave} = 0.815$ and 0.770 under $A = 2.5$ cm and 5 cm respectively. The flat plate has the maximum RAO_{heave} at $\lambda/L = 3.170$ ($f = 0.7$ Hz) with $RAO_{heave} = 0.708$ and 0.711 under $A = 2.5$ cm and 5 cm respectively. Furthermore, RAO_{heave} for the catamaran is larger than that of the flat plate when $\lambda/L = 1.561, 1.927$ and 2.437 and is smaller than that of the flat plate when $\lambda/L = 3.170$ and 2.437, which indicates that the catamaran configuration has smaller heave motion in longer wave cases. For shorter waves, the flat plate is better. The results for both structures with the breakwater in Fig. 6 are presented in Fig. 7(b). It is observed that RAO_{heave} is reduced to lower than 0.4 for all the cases. To more clearly and quantitatively show the influence of the breakwater, take the cases with $A = 5$ cm as an example, the percentage of reduction is calculated and presented in Tables 2 and 3. It can be found that the percentage of reduction is more than 50% for all the cases in addition to that at $\lambda/L = 4.237$. The maximum percentage of reduction for RAO_{heave} is at $\lambda/L = 1.561$ for both the flat plate and the catamaran.

The results of RAO_{pitch} are given in Fig. 8. In Fig. 8(a) for the flat plate, RAO_{pitch} is not sensitive to the incident wave amplitude A, and an obvious difference on RAO_{pitch} is only observed at $\lambda/L = 3.170$ ($f = 0.7$ Hz). By contrast, the pitch motion of the catamaran is quite sensitive to A. This phenomenon is quite similar to that of the heave motion presented in Fig. 7(a). Among the five considered frequencies, the maximum value of RAO_{pitch} occurred at $\lambda/L = 2.437$ ($f = 0.8$ Hz)

for the catamaran, and at $\lambda/L = 3.170$ ($f = 0.7$ Hz) for the flat plate. Besides, the catamaran has a RAO_{pitch} higher than that of the flat plate when $\lambda/L = 1.561, 1.927$ and 2.437, and has a much smaller value when $\lambda/L = 1.561$, which is also similar to the conclusion of the heave motion. The result of the pitch motion after the breakwater is applied is given in Fig. 8(b). It can be seen that RAO_{pitch} is significantly reduced. The typical percentage of the reduction at $A = 5$ cm is given in Tables 4 and 5 respectively. A conclusion similar to the breakwater in the heave motion can be found here. In particular, the reduction of RAO_{pitch} is nearly all larger than 50% except for the case at $\lambda/L = 4.237$ ($f = 0.6$ Hz), and the maximum reduction is at $\lambda/L = 1.561$ ($f = 1.0$ Hz) Hz for both types of structures.

The results of RAO_{surge} are given in Fig. 9. In Fig. 9(a), it is found that RAO_{surge} increases with λ/L in all four cases. RAO_{surge} of the
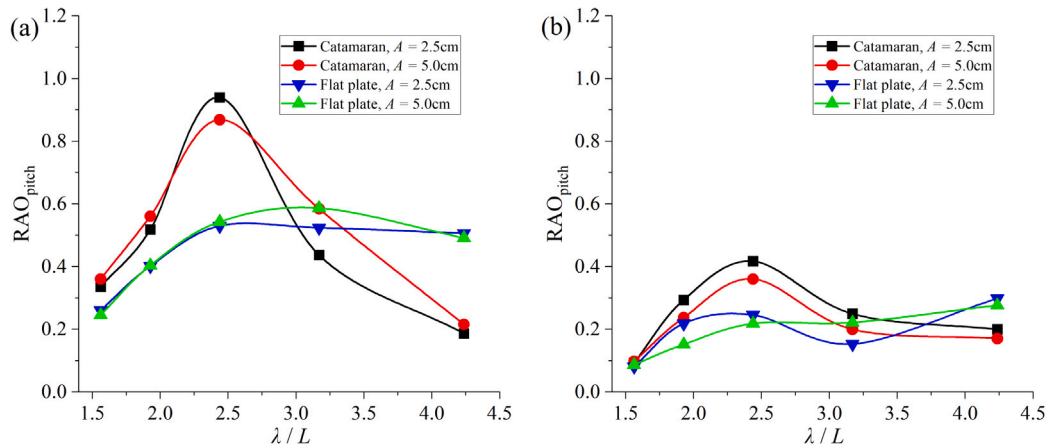
Fig. 8. Pitch motion of the solar panel structures. (a) Without breakwater; (b) With breakwater; Solid lines are the fitted lines from the experimental data.
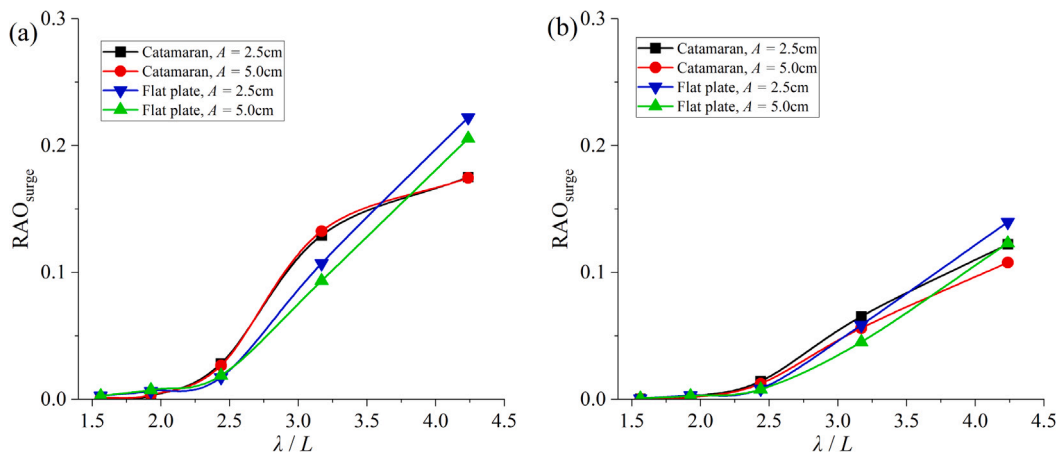

Fig. 9. Surge motion of the solar panel structures. (a) Without breakwater; (b) With breakwater; Solid lines are the fitted lines from the experimental data.

Table 6
The reduction of RAO_{surge} for the flat plate after the breakwater is used under $A = 5$ cm.

λ/L	Without breakwater	With breakwater	Reduction
4.237	0.206	0.123	40.14%
3.170	0.0933	0.0452	51.57%
2.437	0.0187	0.00776	58.50%
1.927	0.00744	0.00262	64.75%
1.561	0.00265	0.000601	77.32%

Table 7
The reduction of RAO_{surge} for the catamaran after the breakwater is used under $A = 5$ cm.

λ/L	Without breakwater	With breakwater	Reduction
4.237	0.175	0.108	38.29%
3.170	0.133	0.0561	57.71%
2.437	0.0266	0.0123	53.76%
1.927	0.00344	0.00131	61.83%
1.561	0.000830	0.000333	59.89%

catamaran structure is not sensitive to the wave amplitude A, and the values of RAO_{surge} under $A = 2.5$ cm and 5 cm at a fixed λ/L are quite close. By contrast, obvious differences can be observed in RAO_{surge} of the flat plate at $\lambda/L = 3.170$ and 4.237 ($f = 0.7$ and 0.6 Hz). The maximum values of RAO_{surge} for both types of structures occur at $\lambda/L = 4.237$, where RAO_{surge} of the catamaran is smaller than that of the flat plate. Once the breakwater is applied, the results of RAO_{surge} are shown in Fig. 9(b). In all cases, it is found that the magnitude of RAO_{surge} reduced to below 0.15. The typical percentage of reductions for the case $A = 5$ cm are summarised in Tables 6 and 7. Similar to the discussion for the heave and pitch motions, here, the reduction on RAO_{surge} is more than 50% for all the cases apart from $\lambda/L = 4.237$ ($f = 0.6$ Hz). The maximum reduction also occurred at $\lambda/L = 1.561$ ($f = 1.0$ Hz) with **77.32%** and **59.89%** for the flat plate and the catamaran respectively.

The wave tank tests reveal that the catamaran structure has better seakeeping ability than the flat plate structure under long wave conditions. This improvement is due to the double-hull design of the catamaran floater, which provides a greater righting moment when a long wave propagates through the structure, and can effectively minimise pitch motion and loads on the mooring system. By contrast, the flat plate performs better under short waves since it blocks the propagation of short waves, while short waves can still pass through the middle gap of the catamaran. However, as the designed breakwater significantly reduces shorter waves, combining the catamaran with a breakwater is deemed to be an effective optimisation strategy.

In addition to the amplitudes of the motions of the structures, we may also present the data of the time history here. In particular, the pitch motion may significantly affect the energy efficiency of FPV. The pitch motion time history $\alpha_y(t)$ versus time t at $\lambda/L = 4.237$ ($f = 0.6$ Hz) and 2.437 ($f = 0.8$ Hz) for the two types of structures
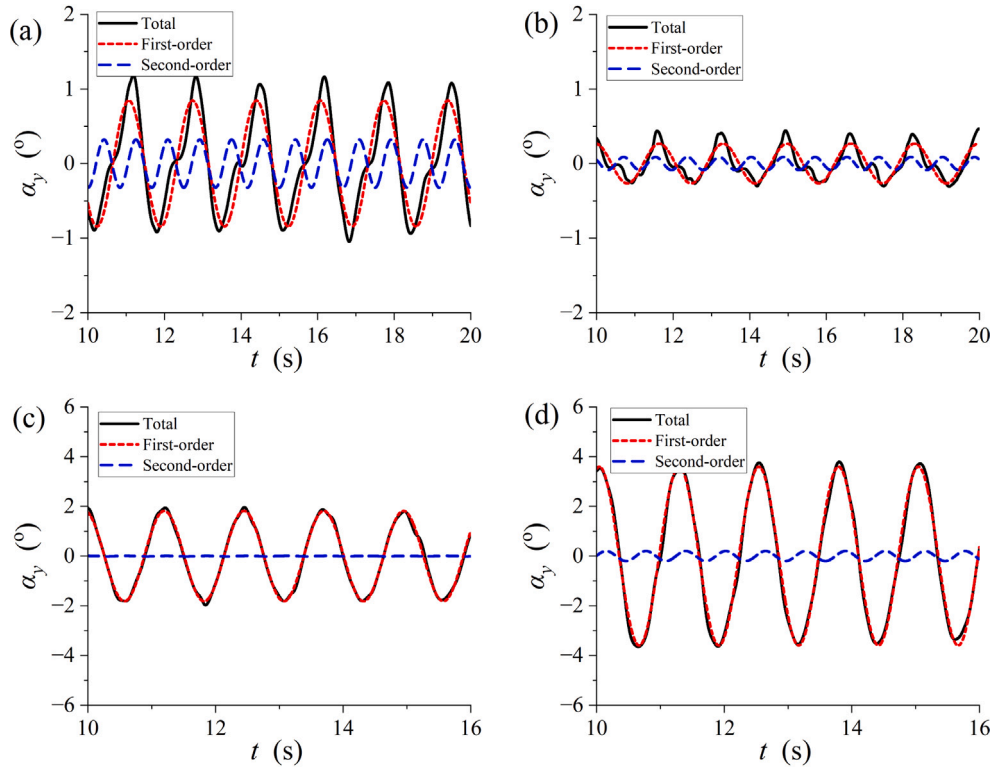
Fig. 10. Time history of the pitch angle of the floating structures without the breakwater, the incident wave amplitude $A = 2.5$ cm. (a) $\lambda/L = 4.237$, flat plate; (b) $\lambda/L = 4.237$, catamaran; (c) $\lambda/L = 2.437$, flat plate; (d) $\lambda/L = 2.437$, catamaran.

Table 8
The amplitudes of the first- and second-order components in α_y for the two types of structures without the breakwater, the incident wave amplitude $A = 2.5$ cm.

Structure type	λ/L	$\alpha_y^{(1)}$ (°)	$\alpha_y^{(2)}$ (°)	$\alpha_y^{(2)}/\alpha_y^{(1)}$
Flat plate	4.237	0.839	0.322	0.384
Flat plate	2.437	1.811	0.00900	0.00497
Catamaran	4.237	0.264	0.0864	0.327
Catamaran	2.437	3.589	0.202	0.0563

Table 9
The amplitudes of the first- and second-order components in α_y for the two types of structures with the breakwater, the incident wave amplitude $A = 2.5$ cm.

Structure type	λ/L	$\alpha_y^{(1)}$ (°)	$\alpha_y^{(2)}$ (°)	$\alpha_y^{(2)}/\alpha_y^{(1)}$
Flat plate	4.237	0.551	0.130	0.236
Flat plate	2.437	0.810	0.188	0.232
Catamaran	4.237	0.168	0.0636	0.379
Catamaran	2.437	1.564	0.0191	0.0122

without the breakwater is given in Fig. 10. In the figure, the first-order and second-order results are computed by applying the Fourier series expansion [45] to the time series data, which is employed to reflect the nonlinearity within the results. Besides, the amplitudes of the first- and second-components $\alpha_y^{(j)}$ ($j = 1, 2$) are summarised in Table 8. From Fig. 10 and Table 8, it can be observed that $\alpha_y^{(2)}/\alpha_y^{(1)}$ is much larger in the case of $\lambda/L = 4.237$ for both types of structures, and the corresponding time history of α_y is deeply affected by the second-order wave components. By contrast, the second-order component in α_y at $\lambda/L = 2.437$ is much weaker, and the first-order component dominates the profiles of the time history. Besides, for both types of structures, although the wave amplitude in the case $\lambda/L = 4.237$ is smaller than that of the $\lambda/L = 2.437$, the nonlinearity in α_y even be stronger. This further reflects the nonlinear wave components still play an important role in the hydrodynamic responses of the present problems. It should be mentioned that the components higher than the second-order are significantly smaller than the first two components, and have little influence on the motions.

The time histories $\alpha_y(t)$ of the two types of structures with the breakwater are shown in Fig. 11, and the corresponding amplitudes of the first- and second-order components are given in Table 9. Similar to Fig. 10, the nonlinearity in α_y is much more obvious at $\lambda/L = 4.237$ ($f = 0.6$ Hz) than that at $\lambda/L = 2.437$ ($f = 0.8$ Hz), or the effect of high-order wave components is much clearer. From Tables 8 and

9, $\alpha_y^{(1)}$ in all cases are effectively reduced by using the breakwater. However, $\alpha_y^{(2)}$ reversely becomes much larger in the case of the flat plate at $\lambda/L = 2.437$. This demonstrates that although the breakwater can effectively reduce the amplitudes of the major wave component, the disturbance of the flow field may increase the high-order response of the motions.

4.2. Mooring forces

The forces in the front side mooring lines are measured through load cells and the corresponding amplitudes F_a are shown in Fig. 12, which is nondimensionalised as $F_a/\rho g L^2 A$, where $\rho = 1000$ kg/m³ denotes the density of the water. The rear side mooring force was not measured as they are considerably smaller than those of the front, and thus not a critical assessment here. In Fig. 12(a), apart from the results at $\lambda/L = 3.170$ ($f = 0.7$ Hz), the values of $F_a/\rho g L^2 A$ under $A = 2.5$ cm and $A = 5.0$ cm are quite close to each other at a fixed λ/L for both types of structures. By contrast, at $\lambda/L = 3.170$, where the maximum mooring line forces occurred for both structures, large differences can be observed in $F_a/\rho g L^2 A$ under two different wave amplitudes. In Fig. 12(b), it can be observed that the magnitude of $F_a/\rho g L^2 A$ is significantly reduced after using the breakwater. Besides, the maximum value of $F_a/\rho g L^2 A$ still remains at $\lambda/L = 3.170$ ($f = 0.7$ Hz). To show the percentage of reduction more clearly, we may take
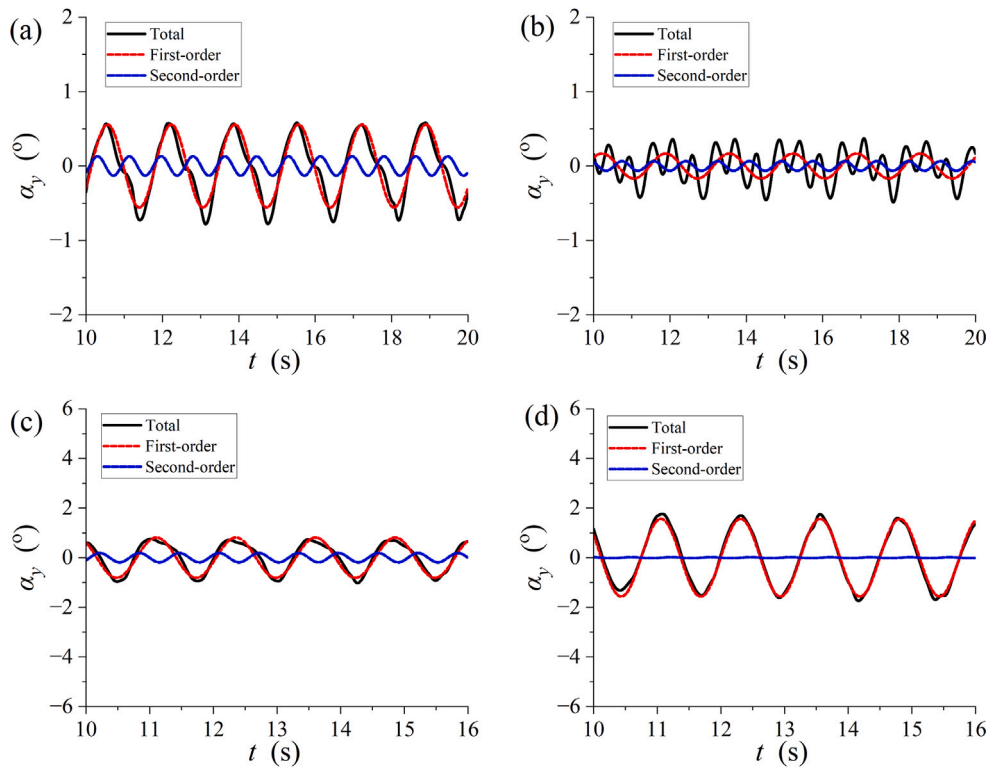
Fig. 11. Time history of the pitch angle of the floating structures with the breakwater, the incident wave amplitude $A = 2.5$ cm. (a) $\lambda/L = 4.237$, flat plate; (b) $\lambda/L = 4.237$, catamaran; (c) $\lambda/L = 2.437$, flat plate; (d) $\lambda/L = 2.437$, catamaran.
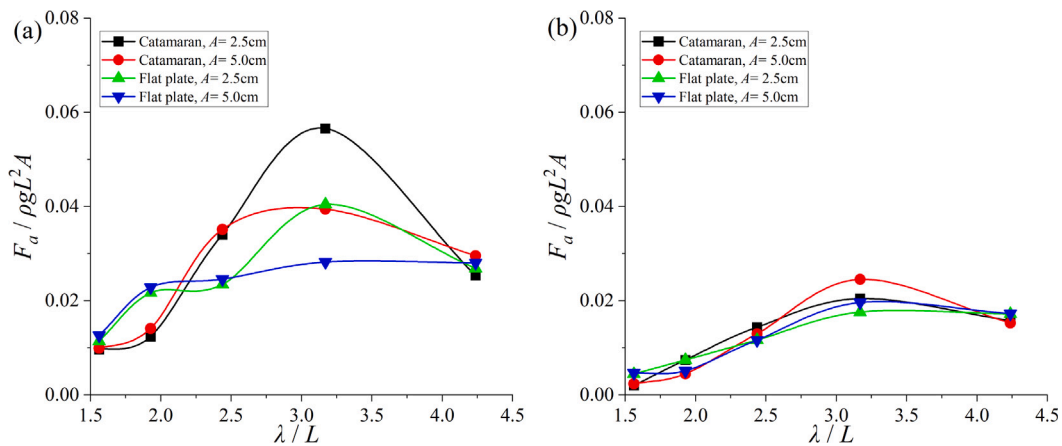

Fig. 12. Force on the front side of the mooring lines. (a) Without breakwater; (b) With breakwater.

$A = 5$ cm as an example, the percentage of the reduction of the mooring line force is given in Tables 10 and 11. It is found that the reduction at $\lambda/L = 4.237$ and 3.170 ($f = 0.6$ and 0.7 Hz) are smaller than 50%, but that at the other three wavelengths are all more than 50%. The maximum reduction occurs at $\lambda/L = 1.927$ ($f = 0.9$ Hz) for the flat plate, and at $\lambda/L = 1.561$ ($f = 1.0$ Hz) for the catamaran.

The time history of the forces $F(t)$ in the front side mooring lines is also analysed. The investigation here focuses on the peak point at $\lambda/L = 3.170$ ($f = 0.7$ Hz) as illustrated in Fig. 12. The results of the cases without the breakwater are given in Fig. 13. One thing here should be noted is that the mean force caused by the initial extension of the mooring line is removed, and thus the present mean value of the time history is at $F = 0$. The Fourier series expansion is also employed here to evaluate the nonlinearity of the results. In Fig. 13, strong nonlinear effects can be observed in the wave trough area in all the presented 4 cases. By applying the Fourier series expansion to the data, it is

Table 10
The reduction of $F_a/\rho g L^2 A$ for the flat plate after the breakwater is used under $A = 5$ cm.

λ/L	Without breakwater	With breakwater	Reduction
4.237	0.0280	0.0172	38.57%
3.170	0.0282	0.0196	30.44%
2.437	0.0246	0.0116	52.71%
1.927	0.0228	0.00512	77.55%
1.561	0.0126	0.00465	63.01%

found that the first several high-order components (2nd, 3rd, 4th) have similar magnitude of amplitudes, and their superposition induces such special features in the wave trough area. The force components higher than 5th are nearly negligible. Besides, the difference in the wave trough is mainly caused by the phase differences of each component.
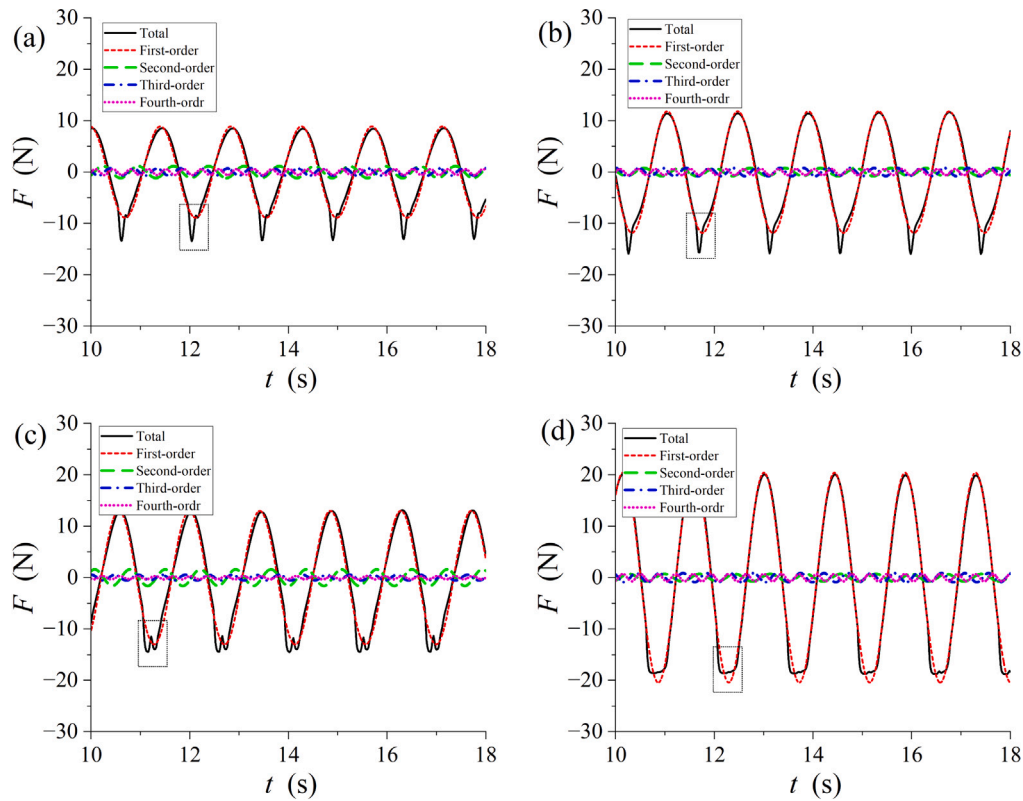
Fig. 13. Time history of the force in the front mooring line at $\lambda/L = 3.170$, without the breakwater. (a) $A = 2.5$ cm, flat plate; (b) $A = 2.5$ cm, catamaran; (c) $A = 5$ cm, flat plate; (d) $A = 5$ cm, catamaran.

Table 11
The reduction of $F_a/\rho g L^2 A$ for the catamaran after the breakwater is used under $A = 5$ cm.

λ/L	Without breakwater	With breakwater	Reduction
4.237	0.0296	0.0153	48.42%
3.170	0.0394	0.0245	37.77%
2.437	0.0351	0.0130	63.09%
1.927	0.0141	0.00449	68.10%
1.561	0.00994	0.00234	76.50%

Hence, Fig. 13(a)~(d) reflect the importance of high-order components in the present problem.

The time histories of the forces at $\lambda/L = 3.170$ after the breakwater is deployed are presented in Fig. 14. In Fig. 14(a) and (b) for $A = 2.5$ cm, it can be seen that the strong nonlinear feature at the wave trough area disappeared for both types of the structures. This is because the amplitudes of higher-order components (more than 2nd) are nearly reduced to 0 after the breakwater is used. By contrast, strong nonlinear features can be still observed at the wave trough area in the case $A = 5$ cm, as shown in Fig. 14(b) and (c), and significant amplitudes can be still observed for the higher-order components.

5. Conclusions

In this work, wave tank experiments were conducted to investigate the hydrodynamic performance of two types of FPV floaters equipped with a four-point mooring system, together with the wave attenuation effect of a breakwater. In total 40 experiments were conducted, as a matrix of 10 wave conditions, 2 floating structures, and 2 scenarios with and without the breakwater. When the breakwater is not deployed, the flat plate shows better hydrodynamic performance in relatively shorter wave conditions, while the catamaran is better in longer wave conditions. In real seas, where waves are highly likely longer than those tested, the catamaran has the potential to outperform the flat plate. With the breakwater deployed, a significant wave reduction of over 50% is observed in most of the tested conditions. This suggests that the catamaran with a breakwater could be a promising solution for FPV in the ocean.

Investigations were also conducted on the nonlinearity in the motions of floating structures and the mooring line forces. By applying the Fourier series expansion, pitch time histories at $\lambda/L = 2.437$ and 4.237 were investigated, showing that high-order components significantly affect the longer wave case. Besides, in the scenario with the breakwater, while the first-order wave amplitude was effectively reduced, the amplitudes of high-order components may increase due to local flow disturbances caused by the breakwater.

The experimental results presented can inform the design and optimisation of FPV structures, enhancing hydrodynamic performance for safe operation and energy efficiency. The results highlight the breakwater's significant potential with FPV. Future work will focus on FPV arrays and more complex wave conditions such as focussed waves. Additionally, the experimental approach here can be applied to other types of FPV floaters to assess their hydrodynamic performance in combination with a breakwater. Moreover, the nonlinear results with high-order loading components can inform fatigue analysis of connection components, aiding in the prediction of structural lifetime and the formulation of maintenance plans.
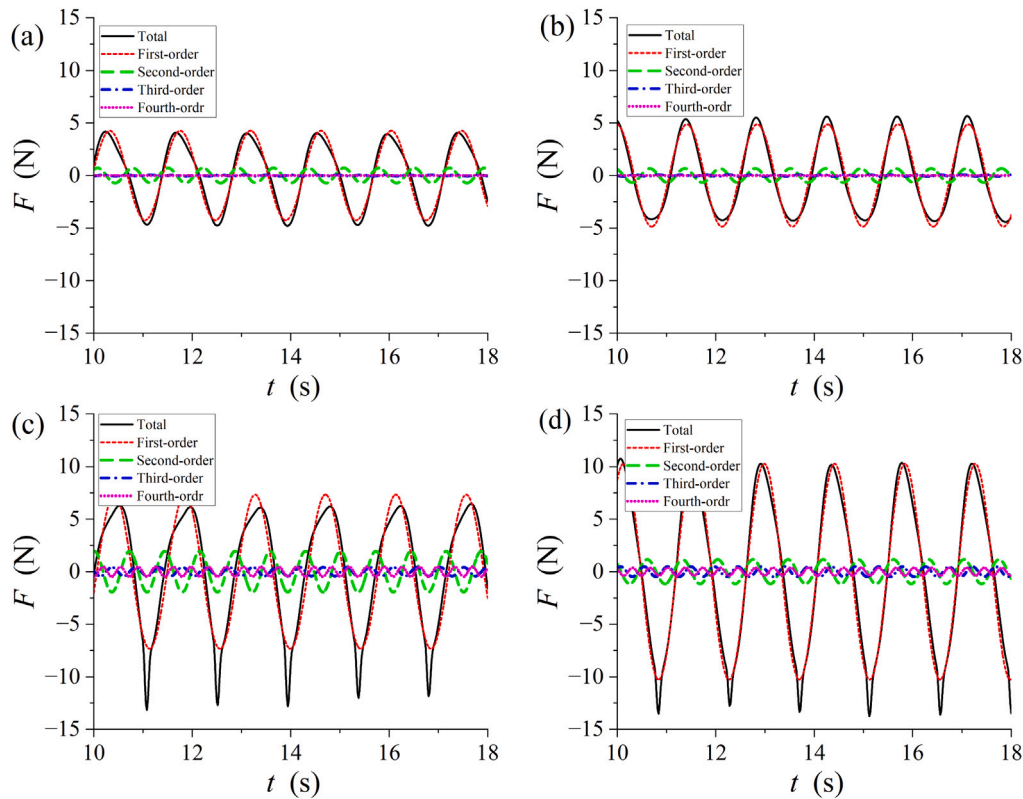
Fig. 14. Time history of the force in the front mooring line at $\lambda/L = 3.170$, with the breakwater. (a) $A = 2.5$ cm, flat plate; (a) $A = 2.5$ cm, catamaran; (c) $A = 5$ cm, flat plate; (d) $A = 5$ cm, catamaran.

CRediT authorship contribution statement

Yifeng Yang: Writing – review & editing, Writing – original draft, Visualization, Formal analysis, Data curation, Methodology. **Chenhao Mi:** Data curation, Formal analysis, Methodology. **Binjian Ou:** Visualization, Data curation, Conceptualization. **Anson Wong:** Writing – review & editing, Resources. **John Gordon Duffy:** Writing – review & editing, Resources. **Tim Wood:** Investigation, Funding acquisition. **IKAP Utama:** Investigation, Funding acquisition. **Wenchuang Chen:** Writing – review & editing, Supervision, Investigation. **Luofeng Huang:** Writing – review & editing, Writing – original draft, Visualization, Supervision, Resources, Project administration, Methodology, Investigation, Funding acquisition, Data curation, Conceptualization.

Declaration of competing interest

The authors declare that they have no known competing financial interests or personal relationships that could have appeared to influence the work reported in this paper.

Acknowledgments

Data availability

All data underlying the results are available as part of the article and no additional source data are required.

References

[1] IEA, World Energy Outlook 2022, Technical Report, 2022.
[2] A. Sahu, N. Yadav, K. Sudhakar, Floating photovoltaic power plant: A review, Renew. Sustain. Energy Rev. 66 (2016) 815–824.
[3] D. Khojasteh, A. Shamsipour, L. Huang, S. Tavakoli, M. Haghani, F. Flocard, M. Farzadkhoo, G. Iglesias, M. Hemer, M. Lewis, et al., A large-scale review of wave and tidal energy research over the last 20 years, Ocean Eng. 282 (2023) 114995.
[4] W. Shi, C. Yan, Z. Ren, Z. Yuan, Y. Liu, S. Zheng, X. Li, X. Han, Review on the development of marine floating photovoltaic systems, Ocean Eng. 286 (2023) 115560.
[5] I. Esparza, Á. Olábarri Candela, L. Huang, Y. Yang, C. Budiono, S. Riyadi, W. Hetharia, R. Hantoro, D. Setyawan, I. Utama, et al., Floating PV systems as an alternative power source: Case study on three representative Islands of Indonesia, Sustainability 16 (3) (2024) 1345.
[6] M. Benghanem, Optimization of tilt angle for solar panel: Case study for Madinah, Saudi Arabia, Appl. Energy 88 (4) (2011) 1427–1433.
[7] A.G. Siraki, P. Pillay, Study of optimum tilt angles for solar panels in different latitudes for urban applications, Solar Energy 86 (6) (2012) 1920–1928.
[8] A.K. Yadav, S.S. Chandel, Tilt angle optimization to maximize incident solar radiation: A review, Renew. Sustain. Energy Rev. 23 (2013) 503–513.
[9] S.Z. Golroodbari, W. van Sark, Simulation of performance differences between offshore and land-based photovoltaic systems, Prog. Photovolt., Res. Appl. 28 (9) (2020) 873–886.
[10] L. Huang, Y. Yang, D. Khojasteh, B. Ou, Z. Luo, Floating solar power loss due to motions induced by ocean waves: an experimental study, Ocean Eng. (2024).
[11] Y. Wei, B. Ou, J. Wang, L. Yang, Z. Luo, S. Jain, W. Hetharia, I. Utama, L. Huang, Simulation of a floating solar farm in waves with a novel sun-tracking system, in: IOP Conference Series: Materials Science and Engineering, IOP Publishing, 2023, 012041.
[12] S. Delacroix, S. Bourdier, T. Soulard, H. Elzaabalawy, P. Vasilenko, Experimental modelling of a floating solar power plant array under wave forcing, Energies 16 (13) (2023) 5198.

[13] C. Zhang, J. Dai, K.K. Ang, H.V. Lim, Development of compliant modular floating photovoltaic farm for coastal conditions, Renew. Sustain. Energy Rev. 190 (2024) 114084.

[14] Y. Wei, S. Yu, P. Jin, L. Huang, K. Elsherbiny, T. Tezdogan, Coupled analysis between catenary mooring and VLFS with structural hydroelasticity in waves, Mar. Struct. 93 (2024) 103516.

[15] Y. Wei, D. Zou, D. Zhang, C. Zhang, B. Ou, S. Riyadi, I. Utama, W. Hetharia, T. Wood, L. Huang, Motion characteristics of a modularized floating solar farm in waves, Phys. Fluids 36 (3) (2024).

[16] M. Rosa-Clot, P. Rosa-Clot, G. Tina, P. Scandura, Submerged photovoltaic solar panel: SP2, Renew. Energy 35 (8) (2010) 1862–1865.

[17] S. Oliveira-Pinto, J. Stokkermans, Assessment of the potential of different floating solar technologies–Overview and analysis of different case studies, Energy Convers. Manage. 211 (2020) 112747.

[18] C. Hu, M. Sueyoshi, C. Liu, Y. Kyozuka, Y. Ohya, Numerical and experimental study on a floating platform for offshore renewable energy, in: International Conference on Offshore Mechanics and Arctic Engineering, Vol. 55423, American Society of Mechanical Engineers, 2013, V008T09A069.

[19] Y.-K. Choi, J.-H. Lee, Structural safety assessment of ocean-floating photovoltaic structure model, Isr. J. Chem. 55 (10) (2015) 1081–1090.

[20] X. Qu, Y. Yao, J. Du, Conceptual design and hydrodynamic performance of a modular hybrid floating foundation, Energies 14 (22) (2021) 7605.

[21] J.-H. Lee, K.-J. Paik, S.-H. Lee, J. Hwangbo, T.-H. Ha, Experimental and numerical study on the characteristics of motion and load for a floating solar power farm under regular waves, J. Mar. Sci. Eng. 10 (5) (2022) 565.

[22] D. Friel, M. Karimirad, T. Whittaker, J. Doran, Experimental hydrodynamic assessment of a cylindrical-type floating solar system exposed to waves, J. Ocean Eng. Sci. 8 (4) (2023) 461–473.

[23] Z. Jiang, J. Dai, S. Saettone, G. Tørå, Z. He, M. Bashir, A. Souto-Iglesias, Design and model test of a soft-connected lattice-structured floating solar photovoltaic concept for harsh offshore conditions, Mar. Struct. 90 (2023) 103426.

[24] A. Abbasnia, M. Karimirad, D. Friel, T. Whittaker, Fully nonlinear dynamics of floating solar platform with twin hull by tubular floaters in ocean waves, Ocean Eng. 257 (2022) 111320.

[25] D.K. Sree, A.W.-K. Law, D.S.C. Pang, S.T. Tan, C.L. Wang, J.H. Kew, W.K. Seow, V.H. Lim, Fluid-structural analysis of modular floating solar farms under wave motion, Sol. Energy 233 (2022) 161–181.

[26] J. van der Zanden, T. Bunnik, A. Cortés, V. Delhaye, G. Kegelart, T. Pehlke, B. Panjwani, Wave basin tests of a multi-body floating PV system sheltered by a floating breakwater, Energies 17 (9) (2024) 2059.

[27] R. Claus, F. Soto, A. Cebada, M. López, D. Clemente, G. Giannini, P. Rosa-Santos, Experimental proof-of-concept of HelioSea: A novel marine floating photovoltaic device, Ocean Eng. 299 (2024) 117184.

[28] S. Timoshenko, S. Woinowsky-Krieger, et al., Theory of Plates and Shells, vol. 2, McGraw-hill New York, 1959.

[29] C. Bi, A.W.-K. Law, Co-locating offshore wind and floating solar farms–effect of high wind and wave conditions on solar power performance, Energy 266 (2023) 126437.

[30] C. Zhang, P. Wang, L. Huang, M. Zhang, H. Wu, D. Ning, Resonance mechanism of hydroelastic response of multi-patch floating photovoltaic structure in water waves over stepped seabed, Phys. Fluids 35 (10) (2023).

[31] Y. Yang, K. Ren, B. Zhou, S.Y. Sun, L. Huang, Wave interaction with multiple adjacent floating solar panels with arbitrary constraints, Phys. Fluids 36 (3) (2024).

[32] Y. Shi, Y. Wei, Z.Y. Tay, Z. Chen, Hydroelastic analysis of offshore floating photovoltaic based on frequency-domain model, Ocean Eng. 289 (2023) 116213.

[33] Z. Li, D. Chen, X. Feng, Hydroelastic and expansibility analysis of a modular floating photovoltaic system with multi-directional hinge connections, Ocean Eng. 289 (2023) 116218.

[34] J. Dai, C.M. Wang, T. Utsunomiya, W. Duan, Review of recent research and developments on floating breakwaters, Ocean Eng. 158 (2018) 132–151.

[35] C. Wang, H. Xu, Y. Zhang, W. Chen, Hydrodynamic investigation on a three-unit oscillating water column array system deployed under different coastal scenarios, Coast. Eng. 184 (2023) 104345.

[36] C. Wang, H. Xu, Y. Zhang, W. Chen, Power capture analysis of a five-unit oscillating water column array integrated into a breakwater in terms of flow field visualization, Energy Convers. Manage. 293 (2023) 117449.

[37] C. Wang, Y. Zhang, H. Xu, W. Chen, Multi-stage wave energy conversion and electric power estimation of a chamber-breakwater integrated system with a U-shaped impulse turbine, Energy Convers. Manage. 313 (2024) 118591.

[38] Y. Wei, S. Yu, X. Li, C. Zhang, D. Ning, L. Huang, Hydrodynamic analysis of a heave-hinge wave energy converter combined with a floating breakwater, Ocean Eng. 293 (2024) 116618.

[39] S.-H. Lee, Y.-G. Lee, S.-H. Kim, On the development of a small catamaran boat, Ocean Eng. 34 (14–15) (2007) 2061–2073.

[40] S.A. Hughes, Physical Models and Laboratory Techniques in Coastal Engineering, vol. 7, World Scientific, 1993.

[41] M. Jifaturrohman, T. Putranto, I. Utama, L. Huang, Effect of platform configurations and environmental conditions on the performance of floating solar photovoltaic structures, in: International Marine Design Conference, 2024.

[42] J. Wittenburg, Dynamics of Systems of Rigid Bodies, vol. 33, Springer-Verlag, 2013.

[43] J.V. Wehausen, E.V. Laitone, Surface waves, in: Fluid Dynamics/StröMungsmechanik, Springer, 1960, pp. 446–778.

[44] L. Huang, G. Thomas, Simulation of wave interaction with a circular ice floe, J. Offshore Mech. Arct. Eng. 141 (4) (2019) 041302.

[45] T.W. Körner, Fourier Analysis, Cambridge University Press, 2022.